

## The Inhibition Effect of a Novel Mannich Base on the Corrosion of A3 Mild Steel in 1.0 M Hydrochloric Acid Solution

Juan Wang<sup>1</sup>, Shi-Ai Xu<sup>1,2,\*</sup>

<sup>1</sup> Shanghai Key Laboratory of Advanced Polymeric Materials, School of Materials Science and Engineering, East China University of Science and Technology, Shanghai 200237, China

<sup>2</sup> The Chemical Engineering College of Qinghai University, Xining 810016, China

\*E-mail: [saxu@ecust.edu.cn](mailto:saxu@ecust.edu.cn)

Received: 21 November 2015 / Accepted: 28 January 2016 / Published: 1 March 2016

---

A novel inhibitor, 2,6-Dichloro-3-fluoroacetophenonamine (DFAPA), was synthesized by the Mannich reaction between ethylenediamine, paraformaldehyde and 2,6-Dichloro-3-fluoroacetophenone (DFAP), and its inhibition effect on the corrosion of A3 mild steel (MS) in 1.0 M hydrochloric acid solution was examined by weight loss, potentiodynamic polarization, electrochemical impedance spectroscopy (EIS) and scanning electron microscopy (SEM). The inhibition efficiency (%IE) of DFAPA increases with its concentration. The *Tafel* curves show that DFAPA behaves as a mixed-type inhibitor, and the EIS results indicate that the charge-transfer resistance ( $R_{ct}$ ) increases with the concentration of DFAPA. With increasing DFAPA concentration, the apparent activation energy ( $E_a$ ) for the MS dissolution decreased slightly, which could be due to the chemisorption of DFAPA onto the metal surface. In addition, the adsorption of DFAPA on the A3 MS surface obeys Langmuir adsorption isotherm.

---

**Keywords:** mild steel, Mannich base, weight loss, EIS, acid inhibition

### 1. INTRODUCTION

Mild steel (MS) has been extensively used in chemical, petroleum and allied industries for the handling of acids, alkalis, and salt solutions. However, the application of MS is somewhat limited by its susceptibility to corrosion in acid medium [1-3]. Inorganic acids, particularly hydrochloric acid have found various industrial applications, such as the acid cleaning and descaling, industry cleaning, and oil-well acidizing [4-6]. The use of inhibitors is one of the most practical methods to reduce the aggressive attack of the acid on the metal and excessive acid consumption in the cleaning process [7-10]. Organic compounds containing one or more N, S, and O atoms can inhibit the corrosion of

metals (particularly active metals like Fe, Zn, and Mg) in aqueous acid solution, making them the most widely used corrosion inhibitors over the past four decades [11-15]. The adsorption of organic compounds on the metal surface in acid solutions has been shown to be related to one or all of the followings mechanisms [1-6]:

(1) Electrostatic interaction between the negatively charged MS surfaces created by adsorbed anions and the positively charged inhibitor;

(2) Unpaired electrons in the inhibitor molecules coordinated with the metal atoms on the MS surface;

(3)  $\pi$  electrons of the inhibitor molecules interacted with the metal atoms on the MS surface;

A large number of studies have been carried out to determinate the adsorptivity of organic compounds at the metal/solution interface [16-21]. It is known that most organic inhibitors act by adsorption on the surface of metals [15]. Organic substances containing N, S and O atoms can be strongly adsorbed on the MS surface by forming a coordinate bond between the unpaired electrons in N, S and O atoms and the vacant *d*-orbital on the MS surface [22-25]. This could change the structure of the electrical double layer and influence the kinetics of electrochemical reaction, thus protecting the metal from dissolution in acid solution [15, 26].

Most commercial inhibitors contain carbonyls and amines as the essential ingredients [27]. It is reported that the condensation products obtained by the reaction of an amine with one or more active hydrogens, formaldehyde, and a carbonyl compound with active hydrogens adjacent to carbonyl, which are known as Mannich bases, exhibit an inhibition efficiency of > 90% at lower concentrations [15, 24, 27-29].

2,6-Dichloro-3-fluoroacetophenone (DFAP) is a byproduct in the production of a drug intermediate named 2,4-dichloro-5-fluoroacetophenone, and the conversion of such a byproduct into useful compounds or materials has been a matter of environmental concern. Because of the active hydrogen adjacent to carbonyl, DFAP can undergo a Mannich reaction with ethylenediamine and formaldehyde to form a novel acid inhibitor. However, the use of 37% formaldehyde aqueous solution may cause some problems, such as excessive energy consumption and water pollution. A possible solution to these problems is to use paraformaldehyde instead of formalin solution. The object of this study is to develop a novel inhibitor based on DFAP, and then to investigate its inhibition efficiency on the corrosion of MS in 1.0 M HCl solution by using electrochemical impedance spectroscopy (EIS), potentiodynamic polarization, weight-loss, and scanning electron microscopy (SEM).

## 2. EXPERIMENTAL

### 2.1. Specimen composition and dimensions

A3 MS coupons composed of (wt %) 0.17% C, 0.46% Mn, 0.3% Si, 0.045% S, 0.045% P, and balance Fe were used. A3 MS coupons of  $4.0 \times 1.3 \times 0.2$  cm<sup>3</sup> were used for weight loss measurements; coupons of  $1 \times 1 \times 0.2$  cm<sup>3</sup> for SEM observation; and coupons of  $1 \times 1 \times 0.2$  cm<sup>3</sup> which were welded with Cu-wire for electrical connection and embedded in epoxy resin, allowing an area of  $1 \times 1$  cm<sup>2</sup> to be

exposed to the test solution, for electrochemical measurements, respectively [7]. Prior to the experiments, all samples were polished with emery papers of 600, 800, and 1200 grades, then washed in order with anhydrous ethanol, acetone and distilled water, and then desiccated before each measurement as recommended by ASTM standard G31-72.

## 2.2. Preparation of inhibitor

A new inhibitor, 2,6-dichloro-3-fluoroacetophenonalamine (DFAPA), was synthesized by Mannich reaction, which was schematically shown in Fig. 1.

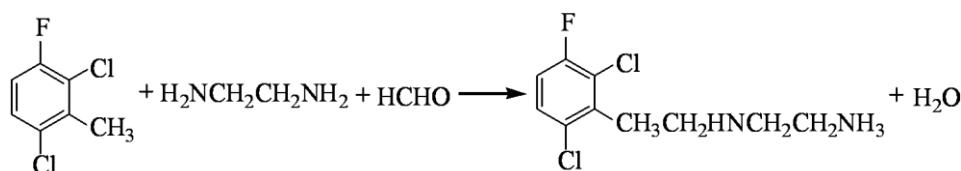


**Figure 1.** Scheme for the synthesis of DFAPA, where the mole ratio of reactants was 1:1:1

Briefly, 82.8 g of 0.2 mol DFAP and 24.0 g of 0.2 mol ethylenediamine were placed in a 250 ml four-necked flask equipped with a magnetic stirrer, a re-flux condenser, and a thermometer, and well-mixed by stirring for 20 min at 333 K. After that, 12 g of 0.2 mol paraformaldehyde was added in 4-5 portions to the reactor over a time period of 40-50 min. After completion of the dissolution of paraformaldehyde, anhydrous ethanol was added to make the reaction mixture to be completely dissolved in the solvent, and then the temperature was raised to 353 K and hatched for 11 h. When the reaction came to an end, the temperature was reduced to 338 K to remove water and anhydrous ethanol by vacuum. The resulted DFAPA was a reddish brown solution.

## 2.3. Test solution

The 1.0 M hydrochloric acid solution was prepared by diluting 37% AR-Grade hydrochloric acid with double distilled water. The concentration of DFAPA was 50, 100, 150, 200, and 300 ppm in hydrochloric acid solution, respectively, and the 1.0 M hydrochloric acid solution without DFAPA was taken as the blank for comparison.

## 2.4. Weight loss measurements

Pre-weighed A3 MS coupons were immersed in 200 mL of 1.0 M HCl solution for 9 h with or without different concentrations (50, 100, 150, 200, and 300 ppm) of DFAPA at 298, 308, 318, 328, and 338 K respectively. Then, the coupons were taken out, washed with double distilled water, wiped with filter paper, dried at room temperature, and then reweighed.

### 2.5. Electrochemical measurements

The potentiodynamic and EIS curves were recorded using a PARSTAT2273 electrochemical workstation with the built-in software. In the experiment, a three-electrode cell consisting of a reference electrode (standard calomel electrode, SCE), a counter electrode (platinum electrode), and a working electrode (A3 MS coated with epoxy resin that allows an area of 1 cm<sup>2</sup> to be exposed to the corrosive medium with or without various concentrations of inhibitor) was used. All potentials were measured versus SCE. The polished and degreased working electrodes were immersed into the acid solution with or without an inhibitor for a while, and the platinum sheet of 1 cm<sup>2</sup> was placed parallel to the working sheet to form an equipotential electric field. In all experiments, the cell was open to atmosphere and the measurements were carried out at 293 K. Before each measurement, the open-circuit potential (OCP) was monitored at 293 K for 60 min in the test solution until reaching a steady state [8]. The potentiodynamic curves were recorded in both cathodic and anodic directions in the electrode potential range from -250 to +250 mV relative to OCP at a rate of 0.5 mV/s potential sweep. EIS was performed at OCP from 100 kHz to 10 mHz, with a peak-to-peak amplitude of 10 mV. The impedance diagrams were presented as Nyquist plots, and the measured impedance curves were fitted using ZSimpWin 3.21.

### 2.6. SEM analysis

As the maximum inhibition efficiency (%IE) was obtained at 300 ppm of DFAPA in 1.0 M hydrochloric acid solution (Table 1), A3 MS coupons were immersed in 1.0 M hydrochloric acid in the absence (blank) and presence of 300 ppm of DFAPA at 318 K for 9 h.

Then, the coupons were taken out, washed with double distilled water, wiped with filter paper, and then dried at room temperature. The SEM images were taken by a HITACHI scanning electron microscope (Model S-4800 FES).

**Table 1.** Effect of DFAPA concentration on the corrosion parameters of A3 MS in 1.0 M HCl at different temperatures from weight loss measurements

Temperature (K)	C (ppm)	$\Delta m$ (g)	$W$ (mg·cm <sup>-2</sup> ·h <sup>-1</sup> )	%IE	$\theta$
298	0	0.1453	1.32	-	-
	50	0.0094	0.09	93.5	0.935
	100	0.0057	0.05	96.1	0.961
	150	0.0055	0.05	96.2	0.962
	200	0.0040	0.04	97.2	0.972
	300	0.0039	0.04	97.3	0.973
308	0	0.2458	2.23	-	-
	50	0.0291	0.26	88.2	0.882
	100	0.0151	0.14	93.8	0.938

	150	0.0124	0.11	95.0	0.950
	200	0.0088	0.08	96.4	0.964
	300	0.0081	0.07	96.7	0.967
	0	0.4010	3.64	-	-
	50	0.0408	0.37	89.8	0.898
318	100	0.0203	0.18	94.9	0.949
	150	0.0150	0.14	96.3	0.963
	200	0.0118	0.11	97.1	0.971
	300	0.0088	0.08	97.8	0.978
	0	0.7273	6.60	-	-
	50	0.2060	1.87	71.7	0.717
328	100	0.0357	0.32	95.1	0.951
	150	0.0211	0.19	97.1	0.971
	200	0.0195	0.18	97.3	0.973
	300	0.0161	0.15	97.8	0.978
	0	1.1730	10.64	-	-
	50	0.4269	3.87	63.6	0.636
338	100	0.0559	0.51	95.2	0.952
	150	0.0272	0.25	97.7	0.977
	200	0.0250	0.23	97.9	0.979
	300	0.0229	0.21	98.0	0.980

### 3. RESULTS AND DISCUSSION

#### 3.1. Weight loss measurements

The weight losses of A3 MS samples immersed in 1.0 M hydrochloric acid solution with or without 50-300 ppm of DFAPA at 298, 308, 318, 328, and 338 K for 9 h are shown in Table 1. Data are presented as mean  $\pm$  standard deviation (SD) of triplicate experiments. It is noted that the SDs vary from 0.01 to 0.66. The inhibition efficiency (%IE) and surface coverage ( $\theta$ ) of various concentrations of DFAPA were calculated from the weight loss data using Eq. (1) and (2), respectively [30]:

$$\%IE = \frac{W_0 - W_i}{W_0} \times 100 \quad (1)$$

$$\theta = \frac{W_0 - W_i}{W_0} \quad (2)$$

where  $W_0$  is the corrosion rate in the absence of DFAPA, and  $W_i$  is the corrosion rate in the presence of various concentrations of DFAPA.

The corrosion rate ( $W$ ,  $\text{mg}\cdot\text{cm}^{-2}\cdot\text{h}^{-1}$ ) was calculated from Eq. (3):

$$(W) = \frac{\Delta m}{St} \tag{3}$$

where  $\Delta m$  is the average weight loss (mg),  $S$  is the surface area of the MS samples ( $\text{cm}^2$ ), and  $t$  is the immersion time (h).

Table 1 shows that the inhibition efficiency (%IE) of DFAPA increases to 98% with the increasing DFAPA concentration to 300 ppm, after that a further increase in the concentration of DFAPA results in no significant change in the inhibition efficiency. The results indicate that the inhibitor DFAPA can effectively protect A3 MS from dissolving in this acidic media probably through the adsorption at the MS surface.

The corrosion rate decreases with increasing concentration of DFAPA. Table 1 also shows that the %IE decreases dramatically with increasing temperature in the presence of 50 ppm of DFAPA due to the adsorption of DFAPA molecules on the A3 MS surface, but changes slightly with temperature in the presence of 100-300 ppm of DFAPA, indicating that the adsorption rate of DFAPA molecules is higher than their desorption rate.

### 3.2. Potentiodynamic polarization studies

The potentiodynamic curves of A3 MS in 1.0 M hydrochloric acid solution in the absence and presence of various concentrations of DFAPA at 298, 308, 318, 328, and 338 K are shown in Fig. 2, and potentiodynamic polarization parameters, including corrosion potential ( $E_{\text{cor}}$ ), corrosion current density ( $I_{\text{cor}}$ ), Tafel slopes ( $b_a$ ,  $b_c$ ) and inhibition efficiency (%IE) obtained from the Tafel curves are shown in Table 2. The inhibition efficiency (%IE) was calculated using Eq. (4) [31]:

$$\%IE = \frac{I_{\text{cor}(b)} - I_{\text{cor}(i)}}{I_{\text{cor}(i)}} \times 100 \tag{4}$$

where  $I_{\text{cor}(b)}$  and  $I_{\text{cor}(i)}$  are the corrosion current density in the absence and presence of various concentrations of DFAPA, respectively.

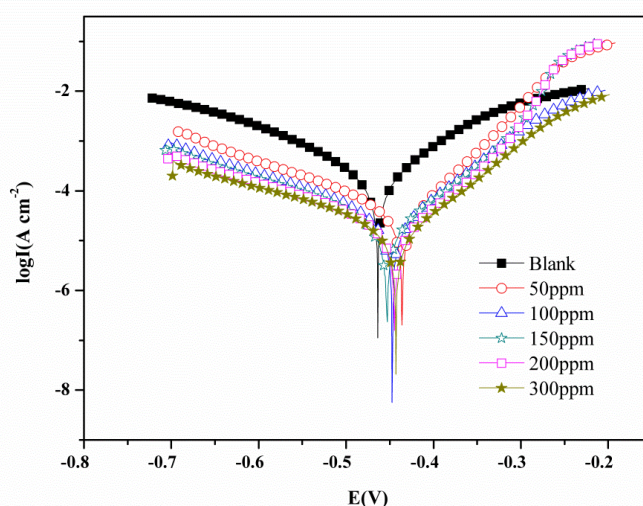


**Figure 2.** The potentiodynamic curves for A3 MS in 1.0 M HCl solution with different concentrations of DFAPA at room temperature

**Table 2.** Electrochemical parameters calculated from the potentiodynamic curves for A3 MS in 1.0 M HCl solution with different concentrations of DFAPA at room temperature

C (ppm)	$E_{\text{cor}}$ (mV)	$I_{\text{cor}}$ ( $\mu\text{A}\cdot\text{cm}^{-2}$ )	$\beta_a$ ( $\text{mV}\cdot\text{dec}^{-1}$ )	$-\beta_c$ ( $\text{mV}\cdot\text{dec}^{-1}$ )	%IE	$\theta$
0	-474	452.0	63	52	-	-
50	-429	39.2	59	168	91.3	0.913
100	-438	28.3	55	121	93.7	0.937
150	-434	23.0	53	132	94.9	0.949
200	-426	19.1	50	143	95.8	0.958
300	-423	17.9	46	133	96.0	0.960

Table 2 reveals that the corrosion current density ( $I_{\text{cor}}$ ) decreases considerably with increasing concentration of DFAPA, while the opposite is true for the inhibition efficiency. An organic compound can be defined as an anodic- or a cathodic-type inhibitor when the displacement in corrosion potential,  $\Delta E_{\text{cor}}$ , is larger than 85 mV [9, 24, 31]. It is observed that the  $E_{\text{cor}}$  values shift towards less positive values, and the maximum value of  $\Delta E_{\text{cor}}$  is about 51 mV after the addition of DFAPA (Table 2), thus indicating that DFAPA behaves as a mixed-type inhibitor [32]. In addition, the cathodic *Tafel* slope,  $b_c$ , increases from 52 to 133 mV/dec; while the anodic *Tafel* slope,  $b_a$ , decreases from 63 to 46 mV/dec with increasing concentration of DFAPA, which further confirms that DFAPA behaves as a mixed-type inhibitor [26, 33]. As the increase in  $b_c$  is obviously higher than the decrease in  $b_a$ , DFAPA appears to have a stronger influence on the kinetics of the hydrogen evolution reaction than on that of the anodic dissolution reaction. The inhibition efficiency (%IE) increases up to 96.0% with the increase of concentration of DFAPA to 300 ppm. The similar phenomenon has also been observed for MS in 1.0 M sulfuric acid solution containing 1((Cyclohexylamino)methyl)urea Mannich base and in 1.0 M hydrochloric acid solution with 2,2',2''((1,3,5-triazine-2,4,6-triyl)tris(azanediyl)tris(methylene)tris-(azanediyl)triethanol (INH-1) [24, 28].

### 3.3. Electrochemical impedance spectroscopy measurements

EIS was performed as an independent and complementary technique to estimate corrosion rates in a rapid and precise way. It also provides an insight into the kinetics of electrochemical processes and the inhibition modes occurring at the MS/acid solution interface modified by DFAPA. Fig. 3 shows the Nyquist plots of A3 MS in 1.0 M hydrochloric acid solution in the absence or presence of various concentrations of DFAPA at room temperature. It is obviously that all the Nyquist plots of A3 MS in uninhibited and inhibited solutions are single depressed capacitive semicircle rather than perfectly circular, indicating that the corrosion process is mainly controlled by the charge transfer process and the resultant double layer behavior.

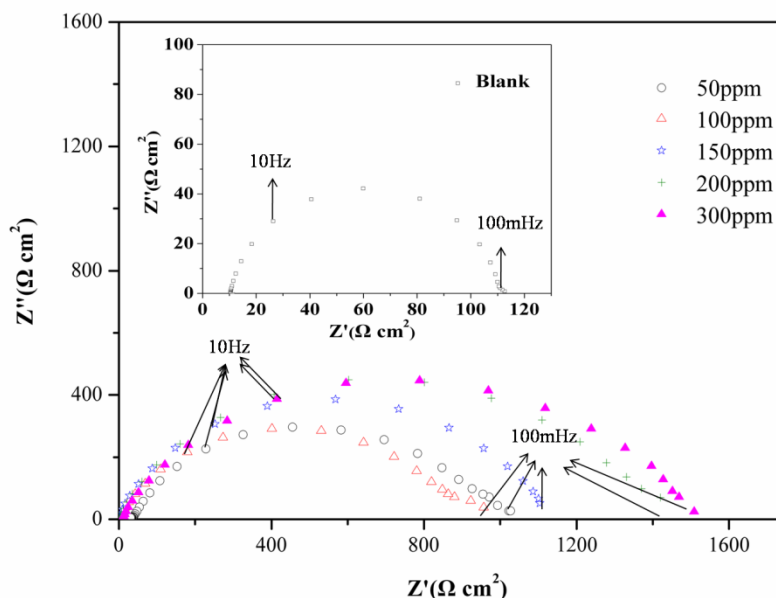


**Figure 3.** The EIS curves for A3 MS in 1.0 M HCl solution with different concentrations of DFAPA at room temperature

The charge transfer resistance ( $R_{ct}$ ) is consistent with the corrosion reaction at the MS surface/solution interface, which is a measurement of electron transfer across the surface and is proportional to the corrosion rate [33]. This can be attributed to the nonhomogeneity of the surface of the working electrode resulting from surface roughness or interfacial phenomena [34]. Although these Nyquist plots are similar to each other in shape, the diameters of these Nyquist plots increase significantly with increasing concentration of DFAPA. An excellent fit with this mode is obtained for all experimental data [33].

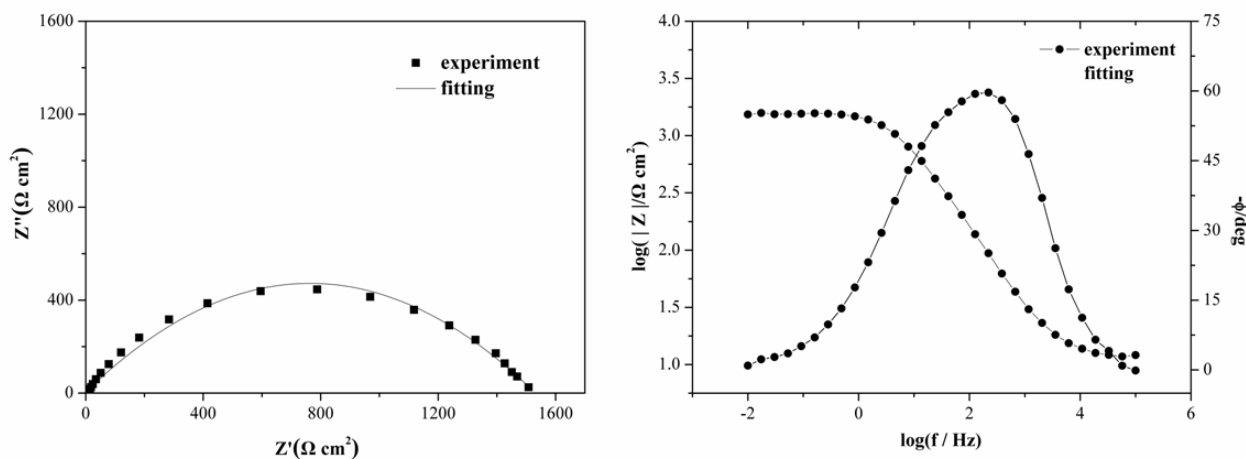


**Figure 4.** Experimental data and best fitting results for EIS (Nyquist and Bode plots) for A3 MS in 1.0 M HCl solution in the absence of 300 ppm of DFAPA

The Nyquist and Bode plots of experimental and fitted data of A3 MS in 1.0 M hydrochloric acid solution containing 300 ppm of DFAPA are shown in Fig. 4, and the Randle’s equivalent circuit for this system is shown in Fig. 5, where  $R_s$  is the resistance of the test solution,  $R_{ct}$  is the charge-transfer resistance, and  $C_{dl}$  is the double-layer capacitance, respectively.

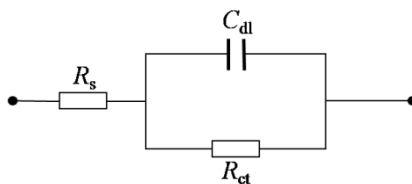


**Figure 5.** The equivalent circuit model

The inhibition efficiency (%IE) was calculated using Eq. (5) [35]:

$$\%IE = \frac{R_{ct(i)} - R_{ct(b)}}{R_{ct(i)}} \times 100 \tag{5}$$

where,  $R_{ct(b)}$  and  $R_{ct(i)}$  are the charge-transfer resistance in the absence and presence of DFAPA, respectively.

The double-layer capacitance ( $C_{dl}$ ) was calculated using Eq. (6):

$$C_{dl} = \frac{1}{2\pi f_{max} R_{ct}} \tag{6}$$

where,  $f_{max}$  is the frequency at the maximum on the Nyquist plot.

**Table 3.** Electrochemical parameters obtained from the EIS plots for A3 MS in 1.0 M HCl solution with different concentrations of DFAPA at room temperature

C (ppm)	$R_{ct}$ ( $\Omega \cdot \text{cm}^2$ )	$C_{dl}$ ( $\mu\text{F} \cdot \text{cm}^{-2}$ )	% IE	$\theta$
0	94	43.66	-	-
50	950	13.48	90.1	0.901
100	1050	8.58	91.0	0.910
150	1150	7.62	91.8	0.918
200	1450	6.34	93.5	0.935
300	1528	6.02	93.8	0.938

Table 3 shows the charge-transfer resistance  $R_{ct}$ , double-layer capacitance  $C_{dl}$ , and inhibition efficiency %IE obtained from the Nyquist plots in Fig. 3. It can be seen that the addition of DFAPA results in a significant increase in  $R_{ct}$  and a reduction in  $C_{dl}$ . The increase in  $R_{ct}$  could be attributed to the blocking of active sites by the inhibitor molecular layer formed on the metal surface; while the reduction in  $C_{dl}$  may result from the decreasing local dielectric constant and/or the increasing thickness of the electric double layer, indicating that DFAPA molecules work by adsorption at the metal/solution interface [24]. Thus, the increasing inhibition efficiency might be result from the gradual replacement of water molecules by DFAPA molecules adsorbed on the metal surface, which can decrease the extent

of the dissolution reaction. These results are consistent with those obtained from weight loss and potentiodynamic polarization measurements.

### 3.4. Adsorption isotherm

The interaction between DFAPA and A3 MS surface can be described the adsorption isotherm. The adsorption of DFAPA molecules on the MS surface is a substitution process whereby the adsorbed water molecules are being replaced by the DFAPA molecules. To determine the mode of adsorption, various standard adsorption isotherms (i.e., Langmuir, Frumkin and Temkin) were fitted to the weight loss data (Table 1). The results show that the adsorption of DFAPA on the A3 MS surface follows Langmuir adsorption isotherm. When  $C$  (concentration of inhibitor) is plotted against  $C/\theta$ , a straight line can be obtained (Fig. 6).

The slopes of Langmuir adsorption isotherm plots and  $K_{ads}$  could be obtained using Eq. (7) [36]:

$$\frac{C}{\theta} = \frac{1}{K_{ads}} + C \tag{7}$$

where  $C$  is the concentration of DFAPA,  $\theta$  is the degree of surface coverage, and  $K_{ads}$  is the adsorption equilibrium constant.

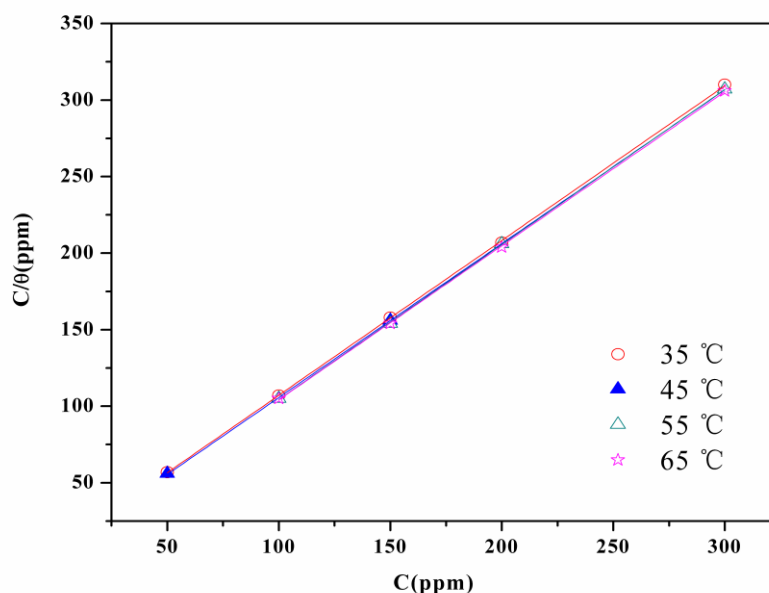


**Figure 6.** Langmuir adsorption isotherms derived from weight loss measurements

Fig. 6 shows that  $C/\theta$  is linearly related to the concentration of DFAPA with correlation coefficients of 0.9999 and slopes of 1.03. Thus the adsorption of DFAPA onto the MS surface obeys Langmuir adsorption isotherm, indicating no interaction between the adsorbed inhibitor molecules [33]. When the surface coverage values approach to 1, a more compact film can be formed depending

on the molecular structure of the inhibitor. The equilibrium constant  $K_{ads}$  can be obtained from the adsorption isotherm, which in turn can be utilized to calculate the standard free energy ( $\Delta G_{ads}$ ) using Eq. (8):

$$\Delta G_{ads} = -RT \ln(55.5K_{ads}) \tag{8}$$

where  $R$  is the gas constant ( $8.314 \text{ J}\cdot\text{K}^{-1}\cdot\text{mol}^{-1}$ ),  $T$  is the absolute temperature (K), the constant 55.5 is the concentration of water in solution expressed in  $\text{mol}\cdot\text{L}^{-1}$ , which is substituted with  $10^6$  ppm to meet the units of  $K_{ads}$ , and  $\Delta G_{ads}$  and  $K_{ads}$  are given in Table 4 at different temperatures.

**Table 4.** Adsorption parameters obtained from Langmuir adsorption isotherms for A3 MS in 1.0 M HCl solution at different temperatures

Temperature (K)	K (ppm <sup>-1</sup> )	$\Delta G_{ads}$ (kJ·mol <sup>-1</sup> )
308	0.17	-30.84
318	0.19	-32.13
328	0.24	-33.78
338	0.28	-35.25

Fig. 7 shows that  $\Delta G_{ads}$  is linearly related to  $T$ , from which the standard adsorption enthalpy and standard adsorption entropy can be derived. The intercept and slope of this plot can be calculated from Eq. (9), then  $\Delta H_{ads} = 14.91 \text{ kJ}\cdot\text{mol}^{-1}$  and  $\Delta S_{ads} = 0.15 \text{ kJ}\cdot\text{mol}^{-1}\cdot\text{K}^{-1}$ , respectively.

$$\Delta G_{ads} = \Delta H_{ads} - T\Delta S_{ads} \tag{9}$$

where  $\Delta H_{ads}$  is the enthalpy of adsorption, and  $\Delta S_{ads}$  is the entropy of adsorption.

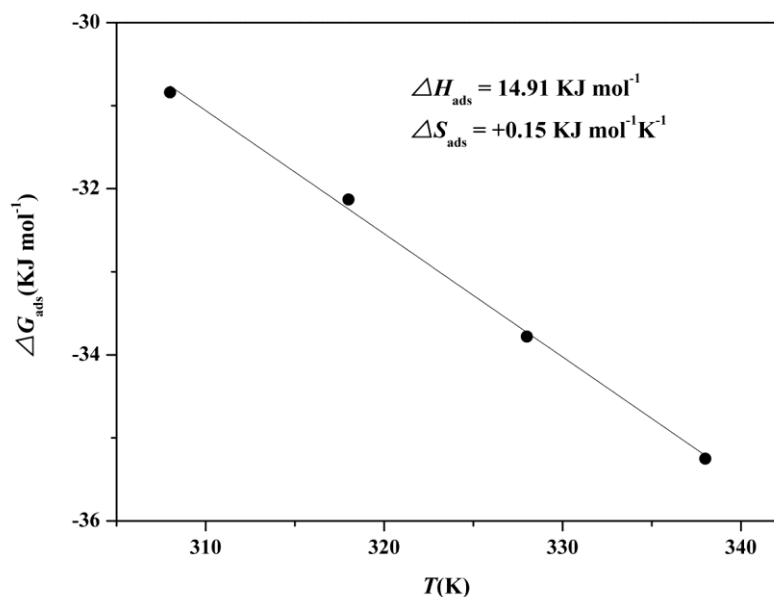


**Figure 7.** Plot of  $\Delta G_{ads}$  vs. T and for the regression straight line and results for the linear-fit parameters

The values of  $\Delta G_{\text{ads}}$  are negative, indicating spontaneous adsorption of DFAPA onto A3 MS surface and strong interactions between DFAPA molecules and A3 MS surface. Generally, the  $\Delta G_{\text{ads}}$  values up to  $-20 \text{ kJ}\cdot\text{mol}^{-1}$  are associated with physisorption (electrostatic interaction between inhibitor molecules and metal), while the  $\Delta G_{\text{ads}}$  values more negative than  $-40 \text{ kJ}\cdot\text{mol}^{-1}$  are associated with chemisorption as a result of sharing or transferring electrons from organic molecules to the MS surface to form a coordinate bond [15, 29].

In the present study, the calculated  $\Delta G_{\text{ads}}$  values range from  $-20$  to  $-40 \text{ kJ}\cdot\text{mol}^{-1}$  (around  $-40 \text{ kJ}\cdot\text{mol}^{-1}$ ), which indicates that the adsorption of DFAPA on the MS surface in acid solution at all temperatures includes both chemisorption and physisorption [37]. The high values of  $|\Delta G_{\text{ads}}|$  suggest a strong interaction between DFAPA molecules and A3 MS surface. It is generally accepted that the physical adsorption is the preceding stage of chemisorption.

The positive values of enthalpy of adsorption ( $\Delta H_{\text{ads}}$ ) imply that this adsorption process is endothermic, indicating that DFAPA is chemically adsorbed. The slight positive change of entropy ( $\Delta S_{\text{ads}}$ ) indicates an increase in randomness as a result of the displacement of adsorbed water molecules from the A3 MS surface [38, 39]. During the chemisorption of inhibitor molecules, a certain number of dissolution may be contained, which creates a net positive entropy change that may be compatible with a slight positive change in enthalpy of adsorption [38]. In conclusion, the weight loss measurement results indicate the occurrence of chemisorption according to a route characterized by a slightly exothermic process with increasing entropy. Thus, DFAPA is a complex mixed-type inhibitor that involves both physisorption and chemisorption.

### 3.5. Influence of temperature

Weight loss measurements were carried out at different temperatures in the absence or presence of various concentrations of DFAPA after immersion for 9 h, and the thermodynamic activation parameters such as energy of activation  $E_a$ , entropy of activation  $\Delta S$  and enthalpy of activation  $\Delta H$  for A3 MS in 1.0 M hydrochloric acid solution in the absence and presence of various concentrations of DFAPA at 298, 308, 318, 328, and 338 K were calculated from the Arrhenius plots from Eq. (11) and the transition state Eq. (12):

$$W_{\text{cor}} = K \exp\left(-\frac{E_a}{RT}\right) \quad (10)$$

$$W_{\text{cor}} = \frac{RT}{N_A h} \exp\left(\frac{\Delta S}{R}\right) \exp\left(-\frac{\Delta H}{RT}\right) \quad (11)$$

where  $W_{\text{cor}}$  is the corrosion rate in the absence and presence of DFAPA,  $A$  is the Arrhenius constant,  $E_a$  is the activation energy,  $R$  is the universal gas constant,  $T$  is the absolute temperature,  $N_A$  is the Avogadro's constant,  $h$  is the Planck's constant,  $\Delta S$  is the change in entropy of activation and  $\Delta H$  is the change in enthalpy of activation, respectively.

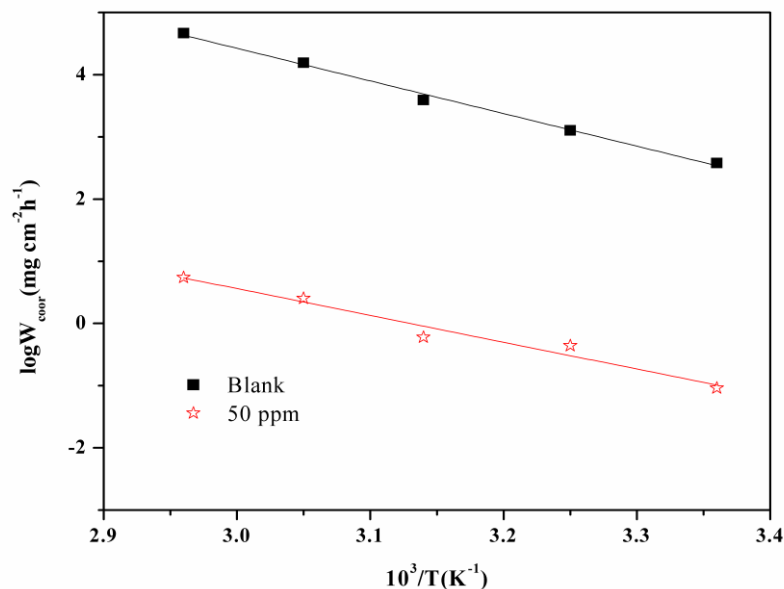


Figure 8. Arrhenius plots of  $\ln(W_{\text{coor}})$  versus  $10^3/T$

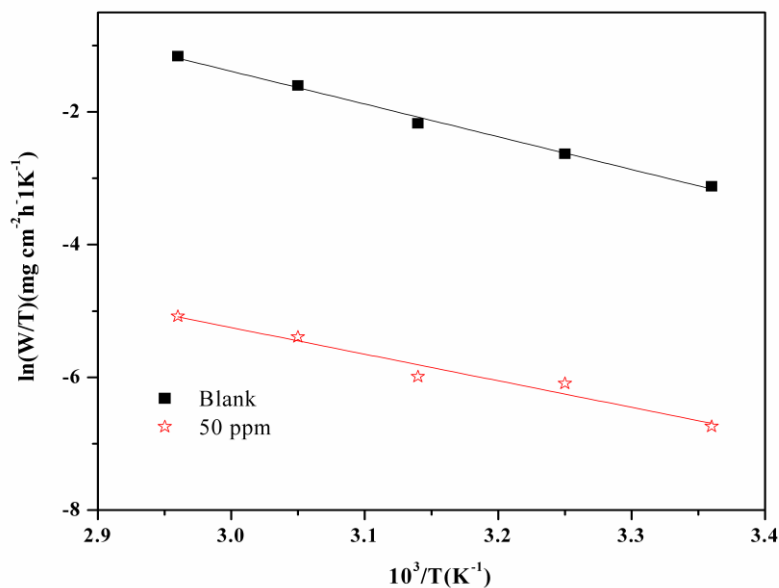


Figure 9. Arrhenius plots of  $\ln(W_{\text{coor}}/T)$  versus  $10^3/T$

The plots of  $\ln(W_{\text{coor}})$  versus  $10^3/T$  (Fig. 8) and  $\ln(W_{\text{coor}}/T)$  versus  $10^3/T$  (Fig. 9) give straight lines with slopes of  $-E_a/R$  and  $-\Delta H/R$  and intercepts of  $A$  and  $[\ln(R/Nh)+(\Delta S/R)]$ , respectively. The activation parameters calculated from the intercepts and slopes are showed in Table 5.

**Table 5.** Activation parameters for A3 MS surface in 1.0 M HCl solution with 50 ppm of DFAPA at different temperatures

Concentration (ppm)	$E_a$ (kJ·mol <sup>-1</sup> )	$\Delta H$ (kJ·mol <sup>-1</sup> )	$\Delta S$ (J·mol <sup>-1</sup> ·K <sup>-1</sup> )
0	43.56	41.00	-105.22
50	79.19	76.64	-108.58

The linear regression coefficients ( $R^2$ ) are very close to 1 in all cases, indicating that the corrosion of A3 MS in 1.0 M hydrochloric acid with or without DFAPA is an activation controlled process. The activation energy of the dissolution reaction of A3 MS in 1.0 M hydrochloric acid solution in the presence of DFAPA is higher than that in the absence of DFAPA [37, 40], which indicates that A3 MS is not easily dissolved in inhibited solution due to the adsorption of DFAPA molecules. The positive sign of enthalpies suggests that the dissolution of A3 MS is an endothermic process [11, 12].

The negative entropy of activation ( $\Delta S$ ) in the presence and absence of DFAPA implies that the activated complex represents a rate-determining step in regard to the association rather than the dissociation step, and a decrease in the disorder occurs when proceeding from reactants to activated complexes [40]. Furthermore, the less negative value of  $\Delta S$  in the presence of DFAPA implies that the presence of DFAPA creates a near-equilibrium corrosion system.

### 3.6. Surface analysis

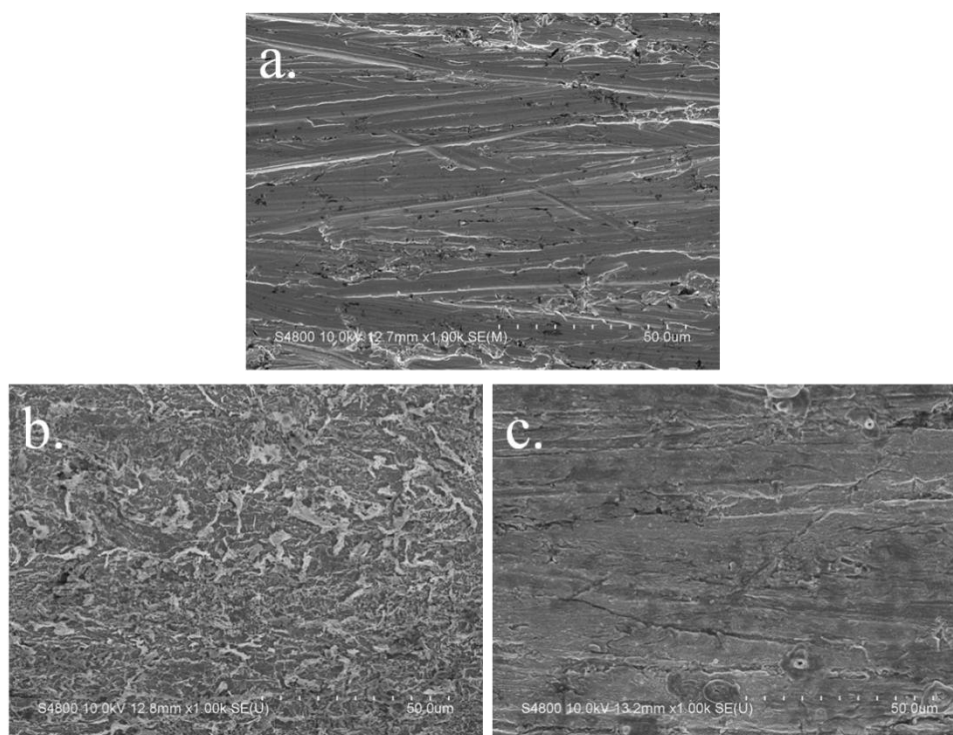
**Figure 10.** SEM micrographs of untested A3 MS (a) and coupons in 1.0 M HCl solution without (b) and with DFAPA (c)

Fig. 10 shows the SEM micrographs of untested A3 MS sample (a) and A3 MS samples immersed in 1.0 M hydrochloric acid solution in the absence (b) and presence (c) of 300 ppm of DFAPA at 298 K for 9 h, respectively. Fig. 10b shows that A3 MS has a very rough surface in acidic solution, which is characteristic of uniform corrosion. Thus the MS surface is completely damaged due to the corrosion in the acidic environment. Fig. 10c shows a smooth surface, which indicates that DFAPA has been adsorbed onto the MS surface to restrict the active sites on the surface [41]. These results corroborate the results obtained by the EIS and weight loss measurements.

#### 4. CONCLUSIONS

The Mannich base DFAPA synthesized in this study could be adsorbed on the MS surface and thus behave as an excellent corrosion inhibitor of A3 MS in 1.0 M hydrochloric acid solution. The weight loss measurement results show that the inhibition efficiency of DFAPA increases to 98% with increasing DFAPA concentration to 300 ppm, decreases with increasing temperature in the presence of 50 ppm of DFAPA but remains stable in the presence of 100-300 ppm of DFAPA. These results are further supported by the potentiodynamic polarization curves, EIS and SEM results. The adsorption of DFAPA on the A3 MS surface follows Langmuir adsorption isotherm. The *Tafel* curves show that DFAPA acts as a mixed-type inhibitor. The standard free energy of adsorption ranges from -20 to -40  $\text{KJ}\cdot\text{mol}^{-1}$ , indicating that the adsorption of DFAPA is both physisorption and chemisorption.

#### ACKNOWLEDGEMENT

This research is financially supported by the National Science Foundation of China (No. 51463020), and the Fundamental Research Funds for the Central University.

#### Appendix

$$\text{Eq. (1)} \quad \%IE = \frac{W_0 - W_i}{W_0} \times 100$$

$$\text{Eq. (2)} \quad \theta = \frac{W_0 - W_i}{W_0}$$

$$\text{Eq. (3)} \quad CR(W) = \frac{\Delta m}{St}$$

$$\text{Eq. (4)} \quad \%IE = \frac{I_{cor}(b) - I_{cor}(i)}{I_{cor}(i)} \times 100$$

$$\text{Eq. (5)} \quad \%IE = \frac{R_{ct}(i) - R_{ct}(b)}{R_{ct}(i)} \times 100$$

$$\text{Eq. (6)} \quad C_{dl} = \frac{1}{2\pi f_{max} R_{ct}}$$

$$\text{Eq. (7)} \quad \frac{C}{\theta} = \frac{1}{K_{ads}} + C$$

$$\text{Eq. (8)} \quad \Delta G_{ads} = -RT \ln(55.5 K_{ads})$$

$$\text{Eq. (9)} \quad \Delta G_{ads} = \Delta H_{ads} - T \Delta S_{ads}$$

$$\text{Eq. (10)} \quad W_{cor} = K \exp\left(-\frac{E_a}{RT}\right)$$

$$\text{Eq. (11)} \quad W_{cor} = \frac{RT}{N_A h} \exp\left(\frac{\Delta S}{R}\right) \exp\left(-\frac{\Delta H}{RT}\right)$$

**References**

1. P. Thiraviyam, K. Kannan, P. Premkumar, *Journal of Chemistry*, 2013 (2013) Article ID 370821
2. S.L.A. Kumar, M. Gopiraman, M.S. Kumar, A. Sreekanth, *Ind. Eng. Chem. Res.*, 50 (2011) 7824-7832.
3. H. Vashisht, S. Kumar, I. Bahadur, G. Singh, *Int. J. Electrochem. Sci.*, 8 (2013) 684-699.
4. M.J. Bahrami, S.M.A. Hosseini, *Int. J. Ind. Chem.*, 3 (2012) 1-9.
5. L.Y.S. Helen, A.A. Rahim, B. Saad, M.I. Saleh, P.B. Raja, *Int. J. Electrochem. Sci.*, 9 (2014) 830-846.
6. G.Y. Elewady, H.A. Mostafa, *Desalination*, 247 (2009) 573-582.
7. M. Behpour, G. S.M, M. Khayatkashani, N. Soltani, *Mater. Chem. Phys.*, 131 (2012) 621-633.
8. Z. Tao, W. He, S. Wang, G. Zhou, *Ind. Eng. Chem. Res.*, 52 (2013) 17891-17899.
9. A. I.O., M. I.C., O. O., E.E. Oguzie, *Int. J. Appl. Sci. Eng. Res.*, 3 (2014) 241-256.
10. A.Khadraoui, A. Khelifa, H. Boutoumi, H. Hamitouche, R. Mehdaoui, B. Hammouti, S.S. Al-Deyab, *Int. J. Electrochem. Sci.*, 9 (2014) 3334-3348.
11. A.K. Singh, *Ind. Eng. Chem. Res.*, 51 (2012) 3215-3223.
12. D.K. Yadav, M.A. Quraishi, *Ind. Eng. Chem. Res.*, 51 (2012) 8194-8210.
13. C. Loganayagi, C. Kamal, M.G. Sethuraman, *ACS Sustain. Chem. Eng.*, 2 (2014) 606-613.
14. M. A. Quraishi, H. K. Sharma, *Mater. Chem. Phys.*, 78 (2002) 18-21.
15. A. K. Singh, M. A. Quraishi, *J. Appl. Electrochem.*, 40 (2010) 1293-1306.
16. P. Mourya, S. Banerjee, M. M. Singh, *Corros. Sci.*, 85 (2014) 352-363.
17. H. Wang, L. K. Ju, H. Castaneda, G. Cheng, B. M. Zhang, *Corros. Sci.*, 89 (2014) 250-257.
18. D. Jayaperumal, *Mater. Chem. Phys.*, 119 (2010) 478-484.
19. G. Chen, H. J. Su, Y. P. Song, Y. Gao, J. Zhang, X. J. Hao, J. R. Zhao, *Res. Chem. Intermed.*, 39 (2013) 3669-3678.
20. B. M. Mistry, A. Jauhari, *Chem. Eng. Commun.*, 201 (2014) 961-981.
21. E. E. Oguzie, M. A. Chidiebere, K. L. Oguzie, C. B. Adindu, H. Momoh-Yahaya, *Chem. Eng. Commun.*, 201 (2014) 790-803.
22. S. Kunar, D. Sharma, P. Yadav, M. Yadav, *Ind. Eng. Chem. Res.*, 52 (2013) 14019-14029.
23. D. B. Hmamou, A. Zarrouk, R. Salghi, H. Zarrok, E. E. Ebenso, B. Hammouti, M. M. Kabanda, N. Benchat, O. Benali, *Int. J. Electrochem. Sci.*, 9 (2014) 120-138.
24. P. Thiraviyam, K. Kannan, *J. Iran. Chem. Soc.*, 9 (2012) 911-921.
25. D. B. Hmamou, R. Salghi, A. Zarrouk, *Ind. Eng. Chem. Res.*, 52 (2013) 14315-14327.
26. A. K. Singh, E. E. Ebenso, *Int. J. Electrochem. Sci.*, 9 (2014) 352-364.
27. M. A. Quraishi, I. Ahamad, A. K. Singh, S. K. Shukla, B. Lal, V. Singh, *Mater. Chem. Phys.*, 112 (2008) 1035-1039.
28. C. Verma, M. A. Quraishi, E. E. Ebenso, *Int. J. Electrochem. Sci.*, 8 (2013) 10851-10863.
29. I. Ahamad, R. Prasad, M. A. Quraishi, *Corros. Sci.*, 52 (2010) 1472-1481.
30. K. Zhang, B. Xu, W. Yang, X. Yin, Y. Liu, Y. Chen, *Corros. Sci.*, 90 (2015) 284-295.
31. E. S. Ferreira, C. Giancomelli, F. C. Giacomelli, A. Spinelli, *Mater. Chem. Phys.*, 83 (2004) 129-134.
32. N. Soltani, M. Khayatkashani, *Int. J. Electrochem. Sci.*, 10 (2015) 46-62.
33. A. Zarrouk, B. Hammouti, T. Lakhlifi, M. Traisnel, H. Vezin, F. Bentiss, *Corros. Sci.*, 90 (2015) 572-584.
34. T. F. Souza, M. Magalhaes, V. V. Torres, E. D'Elia, *Int. J. Electrochem. Sci.*, 10 (2015) 22-33.
35. O. Jilani, N. Njah, P. Ponthiaux, *Corros. Sci.*, 89 (2014) 163-170.
36. S. Deng, X. Li, X. Xie, *Corros. Sci.*, 80 (2014) 276-289.
37. X. Zheng, S. Zhang, W. li, M. Gong, L. Yin, *Corros. Sci.*, 95 (2015) 168-179.
38. [M. V. Fiori-Bimbi, P.E. Alvarez, H. Vaca, C.A. Gervasi, *Corros. Sci.*, 92 (2015) 192-199.

39. H. M., A. El-Lateef, *Corros. Sci.*, 92 (2015) 104-117.
40. D. Daoud, T. Douadi, H. Hamani, S. Chafaa, M. Al-Noaimi, *Corros. Sci.*, 94 (2015) 21-37.
41. K. R. Ansari, M. A. Quraishi, A. Singh, *Corros. Sci.*, 95 (2015).

© 2016 The Authors. Published by ESG ([www.electrochemsci.org](http://www.electrochemsci.org)). This article is an open access article distributed under the terms and conditions of the Creative Commons Attribution license (<http://creativecommons.org/licenses/by/4.0/>).